Journal of *Marine Science and Engineering*

MDPI

Article

Shape-Informed Dimensional Reduction in Airfoil/Hydrofoil Modeling

Zahid Masood [1,†], Konstantinos V. Kostas [1,*,†], Shahroz Khan [2] and Panagiotis D. Kaklis [2,3]

[1] Department of Mechanical & Aerospace Engineering, School of Engineering and Digital Sciences, Nazarbayev University, Kabanbay Batyr Ave. 53, Astana 010000, Kazakhstan; zahid.masood@nu.edu.kz
[2] Department of Naval Architecture, Ocean and Marine Engineering, University of Strathclyde, Glasgow G4 0LZ, UK; shahroz.khan@strath.ac.uk (S.K.); panagiotis.kaklis@strath.ac.uk (P.D.K.)
[3] Foundation for Research & Technology Hellas (FORTH), Institute of Applied & Computational Mathematics (IACM), Division of Numerical Analysis & Computational Science, Group of Data Science, GR 700 13 Heraklion, Crete, Greece
* Correspondence: konstantinos.kostas@nu.edu.kz
† These authors contributed equally to this work.

Abstract: Parametric models have been widely used in pertinent literature for reconstructing, modifying and representing a wide range of airfoil and/or hydrofoil profile geometries. Design spaces corresponding to these models can be exploited for modeling and profile-shape optimization under various performance criteria. Accuracy requirements, along with the need for modeling local features, often lead to high-dimensional design spaces that hinder the process of shape optimization and design through analysis. In this work, we propose a shape-informed dimensional reduction approach that attempts to tackle this deficiency by producing low-dimensional latent design spaces that can be efficiently used in shape representation and optimization. Furthermore, geometric moments are introduced in an attempt to cost-effectively capture analysis-relevant information that is generally expensive to produce. Specifically, geometric integral properties, although intrinsic features of the shape, are quite commonly related to performance indicators employed in performance optimization and therefore provide a cost-effective physics-informed component in the description of the design in the latent space. To this end, we employ the generalized Karhunen-Loève expansion to produce a shape- and physics-informed subspace retaining the highest possible geometric variance and robustness, that is, a lack of invalid designs. At the same time, a series of shape discretizations, encoding the foil's shape profile, are examined with regard to their effect on the resulting latent space's quality and efficiency. Our results demonstrate a significant reduction in the dimensionality of the original design space while maintaining a high representational capacity and a large percentage of valid geometries that facilitate fast convergence to optimal solutions in performance-based optimization.

Keywords: shape-informed parametrization; dimensionality reduction; airfoils; hydrofoils

Citation: Masood, Z.; Kostas, K.V.; Khan, S.; Kaklis, P.D. Shape-Informed Dimensional Reduction in Airfoil/Hydrofoil Modeling. *J. Mar. Sci. Eng.* **2023**, *11*, 1851. https://doi.org/10.3390/jmse11101851

Academic Editor: Md Jahir Rizvi

Received: 18 August 2023
Revised: 11 September 2023
Accepted: 16 September 2023
Published: 23 September 2023

1. Introduction

Free-form functional surfaces, such as wings, rudders, turbine blades, ship hulls, etc., play a vital role in the performance of a wide range of engineering products. Consequently, they have a significant impact on energy efficiency, the environmental footprint, along with structural integrity, safety, durability, and the financial viability of such endeavors. Such surfaces commonly possess complex geometries, which go far beyond simple primitive shapes, and therefore require advanced modeling techniques, e.g., parametric modeling, to efficiently represent and handle their free-form nature. Recent advancements in geometric modeling techniques, pioneered by mathematicians, computer scientists, and engineers, have significantly enhanced the capabilities of parametric modeling. This state-of-the-art technology effectively represents intricate shapes encountered in diverse fields such as naval architecture, ocean engineering, turbo-machinery, and automotive design [1,2].

To meet the need for cutting-edge designs, there is an increasing need for global optimization across increasingly wider design spaces with an ever-increasing number of design variables. However, such attempts are commonly hampered by the curse of dimensionality, which degrades the performance of optimization techniques as the dimension of the design space increases [3,4]. The first steps in design space dimensionality reduction involve methods which identify significant factors and variables and eliminate the remaining ones by assigning appropriate constant values; see [5]. However, this approach is obviously simplistic and may fail to yield optimal results as it overlooks the potential importance of variables' interdependency and their effect on optimization; see also [6]. Variance-based sensitivity analysis, employing Sobol indices [7], allows a more nuanced evaluation of the significance of the variables, but requires a statistically significant number of samples and becomes computationally intensive as dimensionality increases. To address such challenges, dimensionality reduction techniques, ranging from principal component analysis to unsupervised learning and feature extraction techniques, that capture essential design space directions while preserving critical features, have been employed [8]. The last family of methods uncovers the underlying structures, enabling efficient optimization and knowledge acquisition.

Similarly, in the context of functional-surface design, high-dimensional simulation-driven design optimization problems can greatly benefit from the application of offline/upfront, design-space dimensionality reduction methods. Such contemporary methods assess the variability present within the design space and subsequently reduce its dimensionality accordingly. Hence, these techniques enable effective dimensionality reduction to be performed prior to initiating the optimization process. Diez et al. [9] introduced a method based on the Karhunen-Loève expansion, also known as proper orthogonal decomposition, to assess shape modification variability and establish a latent space with a reduced dimension for the shape modification vector; see also [10]. Despite the effectiveness of such approaches, they are not without drawbacks. One such drawback pertains to their failure to fully maintain the shape complexity and its underlying geometric structure. As a result, the resulting latent subspaces lack the ability to generate sufficiently diverse and/or valid shapes efficiently when used in shape optimization. This lack of representational capacity and compactness (i.e., shape validity) can hinder the success of the optimizer by spending the majority of the computational budget exploring infeasible or invalid shapes. In addition, these techniques often rely purely on geometric features and lack information related to performance criteria and the physics involved in the design assessment. Therefore, it is pivotal to employ more sophisticated representations that encompass high-level information regarding the shape's structure and physics.

1.1. Proposed Approach

In this work, we propose a methodology for tackling the aforementioned problems. The proposed approach augments the geometric shape description with integral properties, i.e., geometric moments, before constructing the design space of reduced dimension. Geometric moments allow us to capture both the shape structure and performance information, as they are correlated to physical quantities (lift, drag, area, rigidity, etc.) which are assessed during foil optimization. Geometric moments provide important insights into the form, volume distribution, and potential performance characteristics of a design. Specifically, if we borrow the terminology used for central/standardized moments in probability distributions, second moments correspond to variance, third moments to skewness, while fourth moments describe kurtosis. Therefore, we employ second moments for capturing the shape's distribution around its centroid, third moments to encode shape asymmetry, and finally fourth moments to determine "tailedness", i.e., whether significant portions of the shape are far from the centroid or not. Although the inclusion of the actual performance indices, as estimated via appropriate computational analysis, would be preferable, the cost of such simulations is, in most cases, significantly more expensive than the moments' calculation. Hence, constructing a latent space from a combined geometry/moment description

results in a physics-informed, robust, and diverse design space, which can achieve high convergence rates when employed in design optimization.

Finally, as the employed dimensionality reduction approaches require discrete shape descriptions, we systematically study the effect of possible foil discretizations on dimensionality reduction outcomes and the quality of the resulting latent spaces.

1.2. Related Works

Locality preserving projection (LPP) [11] is a well known unsupervised dimensionality reduction method based on feature extraction. It is a linear approximation of another common method known as Laplacian Eigenmaps (LE) [12]. The goal of LPP is to use a linear transformation to project the original data onto a lower-dimensional space while retaining links between the nearest neighbors. In other words, LPP attempts to preserve local relationships and a neighborhood structure during the dimensionality reduction process.

Several variants of LPP have been proposed to address the specific limitations of the original method. One such variant is the *ILLP-L1* [13], where the L_2 norm is replaced with the L_1 norm to enhance robustness. Despite LPP's demonstrated effectiveness across various datasets, it is noteworthy that projection directions in LPP are highly sensitive to the coordinate system used for data points. Surprisingly, a mere rigid translation of data points, i.e., without altering their relative positions, can lead to significant changes in the projection directions determined by LPP. This indicates that LPP lacks the essential property of translation invariance, which is very significant in our case.

Generative adversarial networks (GANs) have also been used in pertinent literature to model forms of airfoils/hydrofoils. For example, in Chen et al. [14], the authors demonstrated that their approach allowed them to achieve better optimization results with GAN mode shapes than they could with other parameterization techniques. At around the same time, Du et al. in [15] combined a B-spline representation approach with GANs, leading to the creation of BSplineGAN modes for foil design. However, the lack of prior knowledge regarding the proper number of modes to be used is a frequently voiced criticism against such dimension reduction strategies. Shape optimization with these reduced design spaces may fail to produce appropriate results when only a low number of modes is incorporated. On the other hand, using too many modes undermines the benefits gained by dimensionality reduction.

Using validity functions, which successfully eliminate aberrant foil designs, is another method to narrow the design space. This strategy depends on computationally efficient models to constrain the design space rather than reduce the number of design variables. Kedward et al. [16] presented a unique design constraint, based on curve derivatives/curvature, with the goal of ensuring smooth aerodynamic/hydrodynamic shapes during the shape design optimization process. This constraint significantly improved both the optimization's convergence rate and the resulting optimized designs. Li et al. [17] developed a set of marginal functions to represent the link between dominant foil modes and higher-order modes derived from the UIUC [18] database airfoils. These functions effectively eliminated unwanted airfoils from the design space. However, defining acceptable boundaries for curvature-based constraints ahead of time is frequently difficult, and there was no guarantee that the margin-based validity functions did not also eliminate perfectly valid foil designs by accident. Hence, an ideal validity model should be an accurate discriminator of geometric irregularities without the rejection of plausible foil designs.

Li et al. in [19] employed deep learning techniques, including a deep convolutional generative adversarial network (DCGAN) for sampling realistic airfoils and a convolutional (CNN) discriminator to identify abnormal shapes, within a surrogate-based optimization framework for effective aerodynamic shape optimization. However, it is worth noting that the CNN-based validity function may have limitations when it comes to exploring geometric innovation beyond the scope of the UIUC airfoils. This is because the CNN model is trained using the airfoil GAN model, which itself is exclusively pre-trained on UIUC airfoils. Moreover, if the GAN model encounters modal collapse, the geometric

filtering model could potentially exclude conventional airfoil shapes. Consequently, the deep-learning-based filtering model has faced criticism regarding its ability to hinder the discovery of optimal designs with innovative aerodynamic shapes. Jichao Li and Mengqi Zhang [20] introduced a GAN based on the Wasserstein metric (WGAN) to overcome the problem of model collapse observed in the airfoil GAN model. The WGAN-generated synthetic airfoils not only accurately represent the training airfoils but also extend into regions where there is a scarcity of training samples. As a result, the WGAN model demonstrated extrapolation capabilities, enabling it to capture additional geometric information beyond those present in the training set. Very recently, Khan et al. [1] presented an approach that constructs a generic parametric modeler on the basis of a deep convolutional generative adversarial network trained on a large dataset of ship-hull designs which had undergone several of the dimensionality reduction techniques discussed in this work.

2. Materials and Methods

For the application of the proposed dimensionality reduction method, we assume a rich space of foil-profile designs, $\{C\}$, which can be represented/modified by a design vector $\mathbf{v} \in \mathcal{V} \subseteq \mathbb{R}^n$. The design space $\mathcal{V}$ is then defined by an appropriate set of constraints that limit the design space to geometrically and physically valid foil profiles, i.e., $\mathcal{V} := \{\mathbf{v} \in \mathbb{R}^n : g_i(\mathbf{v}) \leq 0,\ i = 1, \ldots, m\}$, where $g_i(\mathbf{v})$, $i = 1, \ldots, m$ correspond to the functional constraints capturing the design requirements. Furthermore, in design optimization, we assume at least one performance metric, e.g., $f : \mathcal{V} \to \mathbb{R}$, which evaluates the performance, $f(\mathbf{v})$, of the corresponding design encoded by $\mathbf{v}$. Therefore, a simplified shape optimization problem targeting the maximization of the performance metric can be stated as:

$$\text{Find } \mathbf{v}^* \in \mathcal{V} : f(\mathbf{v}^*) = \max_{\mathbf{v} \in \mathcal{V}} f(\mathbf{v}). \tag{1}$$

The computational cost of even the simple shape optimization in Equation (1) increases exponentially with the dimension of $\mathcal{V}$, and increases even further when the evaluation of the performance metric, $f(\mathbf{v})$, is complicated and time consuming. In this work, we begin by constructing the initial rich space of foil profile designs, $\{C\}$, with the help of publicly available foil design databases (UIUC foil database; see [18]), and its enrichment with the use of the parametric model described in Section 2.1.1. The details of its construction are discussed in Section 2.1 along with the applied discretization procedures required for the determination of $\mathbf{v}$ and its enrichment with appropriate integral shape properties (geometric moments) in Section 2.2. We conclude this section with a description of the approach followed for the proposed reduction in dimensionality in Section 2.3.

2.1. Design Dataset

Our first attempt to obtain a rich data set was solely based on random foil instances generated using the parametric model described in Section 2.1.1. Specifically, the generation process was initiated with a baseline design vector corresponding to the NACA 2410 foil profile. Subsequently, 5000 random foil designs were generated by modifying the baseline design vector components in the range $\pm 50\%$ of their nominal values. However, the resulting design space proved to be insufficient as it lacked many profile families that are commonly found in pertinent literature. Instead of arbitrarily increasing the number of random designs in hope of reaching a sufficiently rich design space, we instead used, as a basis for our design space, the publicly available UIUC database of foil designs in [18]. This database comprises approximately 1500 foil profiles described by a set of points with varying cardinality. This second approach poses two new problems: the number of foil designs is not sufficiently large, i.e., many gaps exist in the design space, and the profile representation is not only discrete, but it also lacks standardization, i.e., a common number of points or parameters describing each design. We tackle both problems with the same parametric model mentioned above. Specifically, the parametric model allows us to generate a high-accuracy continuous approximation of each foil profile as a NURBS curve,

which can then be discretized, when needed, to any number of points. Additionally, we enrich the design space, by adding variations in each original profile shape. This is easily accomplished by modifying the design vector components in a range around the nominal values ($\pm 5\%$) for each design in the original database. Finally, a design space with 7578[1] unique profile shapes were generated and used in this work.

2.1.1. Employed Parametric Model

In this work, the airfoil/hydrofoil parametric model, firstly introduced in [21] and later extended to cover a wider range of designs in [22], has been extensively used, both for the generation of the original design space, and for providing benchmark shape optimization results; see Section 3. Numerous methodologies have been introduced to address the parametrization of airfoils and hydrofoils in the pertinent literature. A thorough and comparative review of these approaches can be found in the works of Masters et al. [23,24]. We, however, opt to use the parametric model suggested by Kostas et al. in [22] as it is specifically tailored to cater to the unique requisites of design optimization, i.e., a concise set of parameters, in conjunction with a high-fidelity representational capacity for foil profile shapes.

The employed parametric model uses a range of a relatively small number of parameters that limits the dimensions of the design space. Specifically, the baseline parametric model with 11 parameters, presented in [22], can accurately describe a significant percentage (approximately 70%) of the profiles in the UIUC database. The extended parametric models, in the same work, can represent the complete dataset, within Kulfan tolerance, with 15 or 28 parameters, as can be seen in [22,25,26]. Furthermore, it employs parameters with physical meaning (widths, angles, lengths, etc.), which allow users to easily assign values to them, and generates shapes that do not exhibit undesirable oscillations, self-intersections, superfluous inflections points, or any other type of unwanted shape anomaly.

Each model-generated foil instance is represented by a NURBS curve (see [27]) of the order of k defined as follows:

$$\mathcal{C}(t;\mathbf{v}) = (x(t;\mathbf{v}), y(t;\mathbf{v})) := \sum_{i=0}^{n} \mathbf{b}_i(\mathbf{v}) R_{i,k}(t), \quad t \in [t_{k-1}, t_{n+1}], \tag{2}$$

where $\{R_{i,k}(u)\}_{i=0}^{n}$ is the set of rational B-spline basis of order k (degree $= k-1$) defined over the knot sequence, $\{t_0, t_1, t_2, ..., t_{n+k}\}$, and possessing non-negative weights w_i, $i = 0, 1, 2, \ldots, n$, while $\mathbf{b}_i(\mathbf{v})$ are the corresponding control points determined by the parameter vector $\mathbf{v}$. In this work, we use a cubic representation ($k = 4$) with 17 nondimensionalized parameters in $[0, 1]$, and 13 control points ($n + 1 = 13$), as can be seen in Figure 1 and Table 1. Hence, we first find the parameters' values for all designs in the UIUC database and we then enrich the dataset by generating a small number of variations, 5 for each foil profile in the database. Finally, we generate a rich superset of the UIUC database with 7578 foil profiles, represented by continuous cubic NURBS curves, and encoded by 17×7578 parameter values.

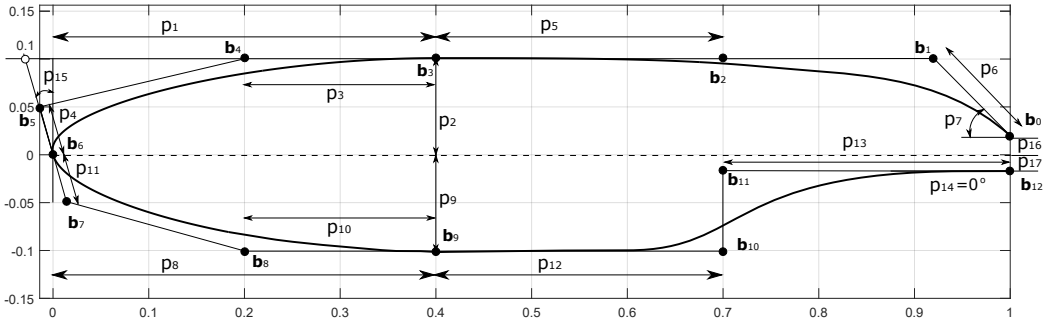

Figure 1. Foil instance of the parametric model employed in this work. The 17 parameters ($p_1, \ldots, p_{17}$) are used for the parametric definition of the 13 control points $\{\mathbf{b}_i\}_{i=0}^{12}$ determining the foil profile.

Table 1. Description of parameters appearing in Figure 1.

No.	Parameter	Description
1	p_1	longitudinal position of maximum upper-side thickness
2	p_2	maximum upper-side thickness
3-4	p_3 & p_4	control of the bulkiness for the front part of the upper side
5-6	p_5 & p_6	shape transition in the back part of the upper side
7	p_7	angle at trailing edge - upper side
8	p_8	longitudinal position of maximum lower-side thickness
9	p_9	maximum lower-side thickness
10–11	p_{10} & p_{11}	control of the bulkiness for the front part of the lower side
12–13	p_{12} & p_{13}	shape transition in the back part of the lower side
14	p_{14}	angle at trailing edge - lower side
15	p_{15}	tangent angle at leading edge
16	p_{16}	ordinate of upper side's endpoint
17	p_{17}	ordinate of lower side's endpoint

2.1.2. Design Discretization

The parametric modeler, as mentioned above, generates continuous curve representations that need to be discretized in the context of the dimensionality reduction techniques used in this work. The discretization in this case converts the continuous curve representation into a polygonal approximation, which can be stored as a vector of point coordinates. From a performance analysis perspective, we need to have a sufficient number of appropriately distributed points on the foil's profile so that the performance evaluation, e.g., drag and lift estimation, produces an identical or insignificantly deviating result. In this work, XFOIL [28,29] was used for foil performance evaluation, and 160 points, with a curvature-based distribution, have been proven in most cases sufficient to produce convergent performance results. However, we need to also account for the effect of the number of points and their distribution in the accurate representation of the dataset that will be used for dimensionality reduction. Specifically, for minimizing the geometric deviation, we pick a higher fixed number of points, i.e., 200, and examine the effect of points distribution by considering the four following cases:

1. ***Uniform spacing over the parametric domain:*** We consider 200 parametric values, $\{t_i\}$ uniformly distributed on the parametric domain, $[t_{k-1}, t_{n+1}]$; see Equation (2). The corresponding 200 points on the profile are used in this case. Note that these 200 points are generally not uniformly distributed on the profile curve; see Figure 2a.
2. ***Cosine spacing:*** We reparameterize the NURBS curve in Equation (2) using the cosine function so that we achieve a concentration of points near the leading and trailing edge; see Figure 2b.
3. ***Curvature-based spacing:*** This approach employs the profile's curvature for calculating the distribution of parametric values. Specifically, parametric points are distributed in a way that guarantees an equal curvature integral for all parametric intervals. This approach results in a large concentration of curve points near the leading edge; see Figure 2c.
4. ***Uniform spacing over the physical domain:*** This approach discretizes the profile by calculating the segments of equal arc-length by dividing the curve length in 199 equal-length curve segments; see Figure 2d.

All aforementioned discretization schemes were applied in the representation of design space and their effect on the dimensionality reduction process and the quality of the latent space produced; see Section 3 for a detailed comparison.

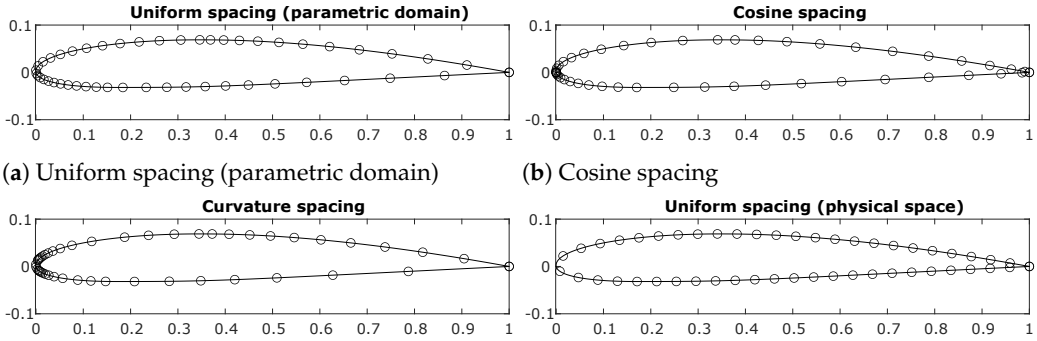

(**a**) Uniform spacing (parametric domain) (**b**) Cosine spacing

(**c**) Curvature-based spacing (**d**) Uniform spacing (physical domain)

Figure 2. NACA 2410 foil discretized using 4 different point distribution schemes. In all cases, 50 points were used.

2.2. Geometric Moments

The common design space dimensionality reduction techniques rely on the geometric representation of the design space (point sets, or polyhedral approximations in the general case) which quite often is insufficient for producing a latent space preserving full shape complexity and the underlying geometric structure. This often leads to subspaces that lack diversity and/or the capacity to generate full valid shapes. Inspired by the research conducted by Khan et al. [10], we augmented the design vectors encoding profile shapes with integral quantities encapsulating high-level shape information. These quantities correspond to geometric moments which, combined with the initial set of point coordinates, construct an enhanced shape signature vector. This enriched representation offers higher levels of accuracy in capturing the shape characteristics while serving as a distinctive signature for the shape itself. Additionally, the presence of geometric moments in the design vector aligns with our second objective of introducing cost-effective approaches to incorporate information on performance metrics. Specifically, as performance metrics, such as lift or drag coefficients, typically require computationally intensive simulations, their correlation to shape information captured by geometric moments enable us to introduce physics-related quantities without the computational burden ensued by CFD simulations. This approach has also been recently demonstrated in [30] for the case of airfoil and hydrofoil performance prediction and optimization where geometric moments have been included as input/output features when training the neural network models presented therein.

We denote by Ω the domain enclosed by the closed curve $\mathcal{C} = \partial\Omega$ which corresponds to our foil profile. We may then calculate the r^{th}-order moments using the following equation:

$$M_{(r)} = M_{p,q} = \int_{-\infty}^{+\infty} \int_{-\infty}^{+\infty} x^p \, y^q \, \rho(x,y) \, dxdy, \quad p,q \in \{0,1,2,\dots\}, \; p+q=r. \tag{3}$$

The quantity $\rho(x,y)$ acquires the value 1 when the corresponding point is in Ω, with the value becoming 0 when $(x,y) \notin \Omega$. When $r = 0$, we retrieve the 2D domain area, i.e., $M_{(0)} = |\Omega|$, and first-order moments can be used for calculating the shape centroid, i.e., $\mathbf{c} = \left(\frac{M_{1,0}}{M_{0,0}}, \frac{M_{0,1}}{M_{0,0}}\right)$. Combining now moments with the design vector comprising point coordinates on the profile, $\mathcal{C} = \partial\Omega$, results in a shape encoding that contains both low and high level geometrical information, while maintaining its uniqueness that permits its use a distinctive identifier or shape a signature vector, as mentioned in [31].

We may obviously compute geometric moments (GMs) in (3) by employing the divergence theorem, i.e., Green's theorem as we are in the 2D case. Therefore, based on Equation (2) which corresponds to our profile NURBS representation, we obtain:

$$
\begin{aligned}
M_{0,0} &= \frac{1}{2}\int_{t_{k-1}}^{t_{n+1}} x(t)\frac{dy(t)}{dt} - y(t)\frac{dy(t)}{dt}dt, \\
M_{1,0} &= \frac{1}{2}\int_{t_{k-1}}^{t_{n+1}} x(t)^2\frac{dy(t)}{dt}dt, & M_{0,1} &= -\frac{1}{2}\int_{t_{k-1}}^{t_{n+1}} y(t)^2\frac{dx(t)}{dt}dt, \\
M_{2,0} &= \frac{1}{3}\int_{t_{k-1}}^{t_{n+1}} x(t)^3\frac{dy(t)}{dt}dt, & M_{0,2} &= -\frac{1}{3}\int_{t_{k-1}}^{t_{n+1}} y(t)^3\frac{dx(t)}{dt}dt, \\
M_{1,1} &= \frac{1}{2}\int_{t_{k-1}}^{t_{n+1}} x(t)^2 y(t)\frac{dy(t)}{dt}dt, & M_{1,1} &= -\frac{1}{2}\int_{t_{k-1}}^{t_{n+1}} y(t)^2 x(t)\frac{dx(t)}{dt}dt,
\end{aligned} \tag{4}
$$

etc.

Finally, an approximate evaluation of the moments appearing in Equations (3) and (4) can be easily accomplished by employing a triangulation of Ω or the discretization of $\partial\Omega \equiv \mathcal{C}(t)$, respectively.

We should also note here that both the lift and drag coefficients, which may serve as performance indicators in this study, are invariant to translational transformations or scaling with a uniform scaling factor. However, the same is not true for the moments in (3) or (4). Hence, employing geometric moments that are invariant to translation and uniform scaling is imperative in this work. Xu and Li in [32] derive translation, scale, and rotation invariant moments (TSR-iGM). For our purposes, rotational invariance is unwanted and therefore, we employ central moments and normalization to achieve translational and scale invariance, respectively. Specifically, by using the centroid of Ω, i.e., $\mathbf{c} = (c_x, c_y) = \left(\frac{M_{1,0}}{M_{0,0}}, \frac{M_{0,1}}{M_{0,0}}\right)$, we obtain the so-called central moments:

$$
\bar{\mu}_{p,q} = \int_{-\infty}^{\infty}\int_{-\infty}^{\infty}(x-c_x)^p(y-c_y)^q\rho(x,y)dxdy. \tag{5}
$$

As for scaling, we can first check its effect on the value of central moments and normalize accordingly. Specifically, if we scale uniformly Ω by a scale factor s, we obtain

$$
\begin{aligned}
\hat{\mu}_{p,q} = &\int_{-\infty}^{\infty}\int_{-\infty}^{\infty}(x-c_x)^p(y-c_y)^q\rho(\frac{x}{s},\frac{y}{s})dxdy = \\
&\int_{-\infty}^{\infty}\int_{-\infty}^{\infty}s^p(x-c_x)^p s^q(y-c_y)^q\rho(x,s)s^2dxdy = s^{p+q+2}\bar{\mu}_{p,q}.
\end{aligned}
$$

We may now use any moment for the normalization, but we pick the 0th order moment since it is easier and more numerically stable to compute, i.e., $\hat{\mu}_{0,0} = s^2\bar{\mu}_{0,0}$. Hence, we can write:

$$
\mu_{p,q} = \frac{\hat{\mu}_{p,q}}{(\hat{\mu}_{0,0})^\ell} = \frac{s^{p+q+2}\bar{\mu}_{p,q}}{(s^2\bar{\mu}_{0,0})^\ell}.
$$

Finally, we set $\ell = \frac{p+q+2}{2}$ to eliminate the scale factor s and we obtain the rth-order normalized central geometric moments

$$
\mu_{(r)} = \mu_{p,q} = \frac{s^{p+q+2}\bar{\mu}_{p,q}}{(s^2\bar{\mu}_{0,0})^{\frac{p+q+2}{2}}} = \frac{\bar{\mu}_{p,q}}{\bar{\mu}_{0,0}^{\frac{p+q+2}{2}}}. \tag{6}
$$

As a side note, one may easily observe that for these TS-invariant moments, $\mu_{(0)} = \mu_{0,0} = \frac{\bar{\mu}_{0,0}}{\bar{\mu}_{0,0}} = 1$, and $\mu_{(1)} = (0,0)$.

2.3. Dimension Reduction

We assume here that our foil geometry corresponds to an appropriate vector of point coordinates $\bar{\boldsymbol{\theta}}$. Additionally, a vector $\mathbf{v} \in \mathcal{V}$ (see Section 2 and Equation (1)) allows one to

define a shape modification procedure: $\bar{\boldsymbol{\theta}}^{\dagger} = \bar{\boldsymbol{\theta}} + \mathbf{v}_{\bar{\boldsymbol{\theta}}}$, where $\bar{\boldsymbol{\theta}}^{\dagger}$ denotes the resulting shape when the modification vector, $\mathbf{v}_{\bar{\boldsymbol{\theta}}}$, is applied to the original shape $\bar{\boldsymbol{\theta}}$.

As previously discussed, the cost of shape optimization increases exponentially with the dimension of $\mathcal{V}$, especially when the performance criteria are many and computationally expensive. To overcome this issue, we propose to use feature extraction techniques to create a lower-dimensional latent-space. As already noted, we also intend to include additional features, i.e., geometric moments, to address some drawbacks of traditional design space dimensionality reduction (DSDR) techniques, and produce a rich latent-space which can be efficiently employed in shape optimization.

To create this latent-space, we combine $\mathbf{v}_{\bar{\boldsymbol{\theta}}}$ with the corresponding geometric moment vector $\boldsymbol{\mu}(\mathbf{v}_{\bar{\boldsymbol{\theta}}})$. We can now define a combined geometry and moment vector $\boldsymbol{p}(\mathbf{v}_{\bar{\boldsymbol{\theta}}}, \boldsymbol{\mu}(\mathbf{v}_{\bar{\boldsymbol{\theta}}})) \in \mathcal{P} \subseteq \mathbb{R}^{n_p}$, where $n_p = n + n_\mu$, with n corresponding to the dimension of $\mathcal{V}$, and n_μ to the number of moments employed. For notational simplicity, we may now define $\boldsymbol{\vartheta} = (\mathbf{v}_{\bar{\boldsymbol{\theta}}}, \boldsymbol{\mu}(\mathbf{v}_{\bar{\boldsymbol{\theta}}}))$ and consequently the function $\boldsymbol{p}(\boldsymbol{\vartheta})$, which encapsulates information about the foil's shape and moments. This function belongs to a disjoint Hilbert space $L^2_f(\mathcal{P})$ defined by a generalized inner product:

$$(\mathbf{a}, \mathbf{b})_f = \int_{\mathcal{P}} f(\boldsymbol{\vartheta}) \mathbf{a}(\boldsymbol{\vartheta}) \cdot \mathbf{b}(\boldsymbol{\vartheta}) d\boldsymbol{\vartheta} = f(\boldsymbol{\mu}_{\bar{\boldsymbol{\theta}}}) \mathbf{a}(\boldsymbol{\mu}_{\bar{\boldsymbol{\theta}}}) \cdot \mathbf{b}(\boldsymbol{\mu}_{\bar{\boldsymbol{\theta}}}) + \int_{\mathcal{V}} f(\bar{\boldsymbol{\theta}}) \mathbf{a}(\bar{\boldsymbol{\theta}}) \cdot \mathbf{b}(\bar{\boldsymbol{\theta}}) d\bar{\boldsymbol{\theta}}, \tag{7}$$

where the inner product is weighted by positive functions $f(\boldsymbol{\mu}_{\bar{\boldsymbol{\theta}}})$ and $f(\bar{\boldsymbol{\theta}})$ that correspond to moments and geometrical description, respectively.

When considering shape optimization in $\mathcal{V}$, one may employ engineers' expert experience and identify regions that could more probably produce the optimum design, i.e., the probability that $\mathbf{v}$ will correspond to the unknown optimum $\mathbf{v}^*$ varies in $\mathcal{V}$. However, as noted in [9,10], when we lack such prior knowledge, we may generally consider a uniform distribution for $\mathbf{v}$, i.e., we consider $\mathbf{v}$ to be an element of a stochastic space $\mathcal{V}$ with an associated probability density function $\rho(\mathbf{v})$, which is uniform in our case. Under this assumption, we can calculate the mean and variance of the signature vector function $\boldsymbol{p}(\boldsymbol{\vartheta})$.

$$\langle \boldsymbol{p} \rangle = \int_{\mathcal{V}} f(\boldsymbol{\vartheta}) \boldsymbol{p}(\boldsymbol{\vartheta}) \rho(\mathbf{v}) d\mathbf{v}, \tag{8}$$

$$\sigma^2 = \langle \|\overline{\boldsymbol{p}}\|^2 \rangle = \int_{\mathcal{V}} \int_{\mathcal{P}} f(\boldsymbol{\vartheta}) \overline{\boldsymbol{p}}(\boldsymbol{\vartheta}) \cdot \overline{\boldsymbol{p}}(\boldsymbol{\vartheta}) \rho(\mathbf{v}) d\boldsymbol{\vartheta} d\mathbf{v}, \tag{9}$$

where $\overline{\boldsymbol{p}}$ is the deviation from the mean, i.e., $\overline{\boldsymbol{p}} = \boldsymbol{p} - \langle \boldsymbol{p} \rangle$.

In dimensionality reduction, we are looking for a lower-dimensional vector $\mathbf{u} \in \mathcal{U} \subseteq \mathbb{R}^\kappa$, with $\kappa << n$, which will substitute $\mathbf{v} \in \mathcal{V} \subseteq \mathbb{R}^n$ in the representation of $\overline{\boldsymbol{p}}(\boldsymbol{\vartheta})$; recall that $\boldsymbol{p}(\boldsymbol{\vartheta}) \equiv \boldsymbol{p}(\mathbf{v}_{\bar{\boldsymbol{\theta}}}, \boldsymbol{\mu}_{\bar{\boldsymbol{\theta}}})$. We now consider this new κ-dimensional vector, the latent variable $\mathbf{u}$, which we want to construct with appropriate features from the original space. Consequently, if the latent space adequately captures the original space, this new latent variable will significantly reduce the computational burden in shape optimization since $\kappa << n$.

Karhunen–Loève Expansion (KLE)

Once the initial shape signature vector (SSV), $\boldsymbol{p}(\mathbf{v}_{\bar{\boldsymbol{\theta}}}, \boldsymbol{\mu}_{\bar{\boldsymbol{\theta}}})$, is constructed to combine shape geometry with invariant geometric moments, we apply the so-called Karhunen–Loève Expansion (KLE) technique to find an appropriate basis of orthonormal functions to approximate our initial space, i.e.,

$$\overline{\boldsymbol{p}}(\boldsymbol{\vartheta}) \approx \sum_{i=1}^{\kappa} u_i \boldsymbol{\phi}_i(\boldsymbol{\vartheta}), \tag{10}$$

where $\{\boldsymbol{\phi}_i(\boldsymbol{\vartheta})\}_{i=1}^{\kappa}$ is the set of the basic functions spanning $\mathcal{U}$, and $\mathbf{u} = (u_1, u_2, \ldots, u_\kappa)$. We obviously want an appropriate latent space $\mathcal{U}$ that will preserve the variance, to the extent possible, exhibited in $\mathcal{P}$. Furthermore, for the components of $\mathbf{u}$, we obtain:

$$u_i = (\overline{\boldsymbol{p}}, \boldsymbol{\phi}_i)_f = \int_{\mathcal{P}} f(\boldsymbol{\vartheta}) \overline{\boldsymbol{p}}(\boldsymbol{\vartheta}) \cdot \boldsymbol{\phi}_i(\boldsymbol{\vartheta}) d\boldsymbol{\vartheta}. \tag{11}$$

Additionally, as mentioned above, we aim to create basic functions that preserve variance σ^2 in the original space; see also Equation (9). If we now plug in Equations (10) and (11) in (9), it is easy to see that:

$$\sigma^2 = \sum_{i=1}^{\infty}\sum_{j=1}^{\infty} \langle u_i u_j \rangle (\boldsymbol{\phi}_i(\boldsymbol{\vartheta}), \boldsymbol{\phi}_i(\boldsymbol{\vartheta}))_f = \sum_{j=1}^{\infty} \left\langle u_j^2 \right\rangle = \sum_{j=1}^{\infty} \left\langle (\overline{\boldsymbol{p}}, \boldsymbol{\phi}_i(\boldsymbol{\vartheta}))_f^2 \right\rangle. \tag{12}$$

As discussed in detail in [9,10], the basis exhibiting the required characteristics can be determined via the solution of the following constrained minimization problem:

$$\min_{\boldsymbol{\phi} \in L_f^2(\mathcal{P})} \left\langle (\overline{\boldsymbol{p}}, \boldsymbol{\phi}(\boldsymbol{\vartheta}))_f^2 \right\rangle,$$
$$\text{subject to:} \quad (\boldsymbol{\phi}(\boldsymbol{\vartheta}), \boldsymbol{\phi}(\boldsymbol{\vartheta}))_f^2 = 1.$$

Finally, as demonstrated in [9,10], this results in

$$\mathscr{L}\boldsymbol{\phi}(\boldsymbol{\vartheta}) = \int_{\mathcal{P}} f(\boldsymbol{\theta}) \langle \overline{\boldsymbol{p}}(\boldsymbol{\vartheta}) \otimes \overline{\boldsymbol{p}}(\boldsymbol{\theta}) \rangle \boldsymbol{\phi}(\boldsymbol{\theta}) d\boldsymbol{\theta} = \lambda \boldsymbol{\phi}(\boldsymbol{\vartheta}), \tag{13}$$

where $\mathscr{L}$, $\otimes$ denotes the self-adjoint integral operator and the outer product, respectively. Both $\boldsymbol{\theta}$ and $\boldsymbol{\vartheta}$ belong to the original space and $\{\lambda\}$ are the eigenvalues. Hence, the resulting eigenvectors $\{\boldsymbol{\phi}_i(\boldsymbol{\vartheta})\}_{i=1}^{\infty}$ correspond to the so-called KL-modes which are orthogonal and constitute the basis of $L_f^2(\mathcal{P})$. Furthermore, the corresponding eigenvalues $\{\lambda_i\}_{i=1}^{\infty}$ represent the variance, i.e.,

$$\sigma^2 = \sum_{i=1}^{\infty} \lambda_i. \tag{14}$$

We now consider the first κ eigenvectors form the basis for our approximation. Obviously, the selection of κ depends on the desired level ε, $(0 < \varepsilon \leq 1)$ of variance we want to capture. In other words, we can choose κ such that the selected eigenvectors capture at least $(\varepsilon \times 100)$ percent of the total variance in the data.

$$\sum_{i=1}^{\kappa} \lambda_i \geq \varepsilon \sum_{i=1}^{\infty} \lambda_i = \varepsilon\sigma^2, \quad \lambda_i \geq \lambda_{i+1}. \tag{15}$$

As a final note, we need to add here that the method described in Diez et al. [9] and Khan et al. [10] is used to numerically solve Equation (13).

2.4. Latent Space

Apart from the dimensionality reduction that leads to the construction of the latent space, as described in Section 3.2, we also need to consider the potential use of parameter bounds which will limit the exploration within a permissible space that lacks, or at least minimizes, the presence of infeasible or invalid designs. This step is quite critical since, although in principle, we want to be able to explore a large space, its size as well as the presence of invalid shapes at some regions constitute hampering factors in the subsequent design optimization. Traditionally, such bounds are defined via functional and/or side constraints that define the feasible design space. In the case of the original design space, the design vector $\mathbf{v}$ commonly comprises parameters with a physical meaning and therefore introducing constraints can be a relatively straightforward task for designers.

However, there are two problems with this approach: the first one stems from the use of the latent space, while the second one pertains to the complexity of the resulting optimization problem. The latter problem is a common problem in constraint optimization where the inclusion of many and/or complicated functional constraints results in a complex and time-consuming optimization problem. Side constraints, i.e., bounds on parameter values, can be more easily handled by the optimization algorithms and are preferred when they can replace the more complicated, usually non-linear, functional constraints. However, the former problem, even when only considering side constraints, remains. Specifically, determining the side constraints, i.e., the parameter bounds $(\mathbf{u}^{low}, \mathbf{u}^{high})$, for the latent space poses additional challenges for designers since $\mathbf{u}$, unlike $\mathbf{v}$, is a latent design vector with no physical meaning, i.e., it does not correspond to lengths, radii, angles, etc. Therefore, as no physical interpretation is generally associated with any component of $\mathbf{u}$, it is difficult to determine the values of $\mathbf{u}^{low}, \mathbf{u}^{high}$, which guarantee that designs within the feasible region of $\mathcal{U}$ are also valid designs in $\mathcal{V}$. In other words, it is difficult to bound $\mathcal{U}$ in a way that will guarantee the satisfaction of all design constraints and the requirements in the original space.

A prevalent method for defining latent space bounds is to utilize the standard deviation from the mean shape, which is positioned at the center of the design space. This method achieves a balance between the number of infeasible shapes and the level of permissible diversity. We consequently follow this approach in our implementation with the bounds of the ith component of the latent variable defines as

$$u_i \in \left[-\sqrt{\alpha\lambda_i}, \sqrt{\alpha\lambda_i}\right], \tag{16}$$

with α being an integer value between 1 and 3, with larger values allowing for larger spaces. In other words, each component of the latent design vector is bounded within a multiple of its deviation.

2.4.1. Latent Space Quality Analysis Measures

To evaluate the appropriateness and effectiveness of a latent space in generating a broad range of diverse and valid shapes, suitable metrics need to be introduced. A commonly used measure of diversity is based on the Hausdorff distance [33], which is frequently employed in the quantification of distance between two subsets of a metric space. Similarly, it can also be employed to quantify the distance, i.e., similarity/dissimilarity, between two free-form shapes. In our case, we assume that both shapes can be appropriately discretized via a corresponding finite set of points, namely $\widehat{C}_1 = \{\mathbf{c}_{1,i} : \mathbf{c}_1 \in \mathbb{R}^2, i = 1, 2, \ldots, n_{C_1}\}$ and $\widehat{C}_2 = \{\mathbf{c}_{j,2} : \mathbf{c}_2 \in \mathbb{R}^2, j = 1, 2, \ldots, n_{C_2}\}$. We can then calculate the Hausdorff distance, H, between the finite sets $\widehat{C}_1$ and $\widehat{C}_2$ as follows:

$$\begin{aligned} H\left(\widehat{C}_1, \widehat{C}_2\right) &= \max\left(h(\widehat{C}_1, \widehat{C}_2), h(\widehat{C}_2, \widehat{C}_1\right), \quad \text{where} \\ h(\widehat{C}_1, \widehat{C}_2) &= \max_{\mathbf{c}_1 \in \widehat{C}_1} \min_{\mathbf{c}_2 \in \widehat{C}_2} \|\mathbf{c}_1 - \mathbf{c}_2\|, \end{aligned} \tag{17}$$

where $h(A, B)$ is the directed Hausdorff distance from A to B, and $\|\cdot\|$ denotes the Euclidean norm. We further assume here that the Hausdorff distance between the two shapes is determined by the Hausdorff distance between the corresponding point sets as defined in Equation (17). Finally, the diversity measure of a latent space is defined as the *mean Hausdorff distance between a reference design and a set of densely sampled designs obtained from the latent space*. Higher values for the diversity measure are desirable as they imply richer latent spaces; however this comes at a cost, i.e., a higher chance of generating invalid geometries. Invalid shapes, in our case, include foils with self-intersections[2], shapes with an oscillatory behavior, foils with upper or lower sides not corresponding to functions[3], etc. Hence, the ideal latent space should not only have a high diversity value but a low or zero percentage of invalid geometries. We define here the validity measure of the latent space as *the ratio of*

invalid designs to valid designs obtained from dense sampling in the latent space. Obviously, a latent space with a validity measure close or equal to 0 is preferred.

2.5. Shape Optimization

After constructing the latent design space, $\mathcal{U}$, an optimization process is carried out to explore its capacity to substitute the original space when searching for optimal designs. We select the lift coefficient, C_L, as the quantity of interest (QoI) for the shape optimization assessment and the corresponding maximization problem can be formulated as follows:

$$\begin{aligned} &\text{Find } \mathbf{u}^* \in \mathcal{U} \quad \text{such that} \\ &\quad C_L(\mathbf{u}^*) = \max_{\mathbf{u}\in\mathcal{U}} C_L(\mathbf{u}) \\ &\text{subject to} \quad |A(\mathbf{u}) - A_0| \leq 0.001, \\ &\qquad\qquad \mathbf{u}^{low} \leq \mathbf{u} \leq \mathbf{u}^{high}, \end{aligned} \tag{18}$$

where A corresponds to the airfoil's area and the sub-index $(_0)$ denotes values for the reference design, i.e., NACA-2410 airfoil. For the above optimization problem, we employ Jaya Algorithm (JA) [34], which is a recently proposed gradient-free, yet effective, meta-heuristic optimization technique, whose excellent performance has been showcased in various engineering applications by different scholars [35–38]. Finally, the lift coefficient is evaluated with the help of the well known XFOIL software package[4], which is a popular tool used in assessing the performance of subsonic airfoils and hydrofoils, as can be seen in [28,29]. One may obviously claim here that the maximization of lift over drag would be a more meaningful performance criterion for the airfoil/hydrofoil shape optimization. However, our intent when performing this shape optimization is for it to serve as a benchmark example for the constructed latent spaces and showcase the differences in their capacity to retrieve optimum geometries and produce a wide range of profile shapes. The competing shape requirements between lift maximization and drag minimization would hinder the clear demonstration of the significant effect discretization and moments' inclusion has on capturing shape information and reproducing or exceeding the optimization results of the original design space and we therefore avoid the use of lift over drag maximization so that we can clearly highlight the differences in the reduced-dimension subspaces.

2.5.1. Jaya Algorithm (JA)

The Jaya algorithm is a widely used population-based optimization technique employed for solving optimization problems. It draws inspiration from social behavior, specifically the concept of individuals within a population enhancing their performance by learning from one another. Initially, a population of potential solutions is randomly generated, with each solution represented as a vector of design variables. Subsequently, the objective function is evaluated for each solution, and the best solution in the population is identified. During each iteration of the Jaya algorithm, the population is updated by considering the current best solution and improving the remaining solutions. This involves adjusting the design variables of each population member towards the current best solution.

The adjustment process in the Jaya algorithm encompasses two fundamental steps: exploration and exploitation. In the exploration phase, each solution within the population undergoes random modifications within a specified range. This enables the algorithm to explore the design space and discover promising new regions. In the exploitation phase, the design variables of each solution are updated based on the current best solution. This facilitates the exploitation of already identified regions that yield improved objective values. The adjustment process is guided by control parameters, such as learning rates and exploration factors, which determine the extent of exploration and exploitation.

The Jaya algorithm iterates until a predefined stopping criterion is met, such as reaching a maximum number of iterations or achieving a desired solution quality level. At the conclusion of the algorithm, the best solution obtained throughout the iterations is

considered the optimal solution to the given optimization problem. The Jaya algorithm has proven successful in solving various optimization problems, including engineering design, scheduling, and parameter tuning. Its simplicity and efficacy have made it a popular choice for addressing real-world challenges; see again [35–38].

3. Results and Discussion

In this section, we present the constructed latent design spaces for different SSVs and shape discretizations, and subsequently compare them with respect to the design space quality metrics introduced in Section 2.4.1. Finally, we demonstrate the use of these latent spaces in performance-based shape optimization, and assess their appropriateness and capacity to reconstruct and/or improve optimal designs.

3.1. Geometric Moment Invariants in SSVs

Although it is possible to calculate geometric moments invariants of any order using the formulation presented in Section 2.2, high-order geometric moments are susceptible to noise [39] and may therefore be easily affected by numerical inaccuracies [31] in their calculation. Moreover, a review of the literature across different fields, such as kinetic equations [40] and shape retrieval [32], indicates that moments of order higher than four are rarely beneficial. We therefore have limited our study to geometric moment invariants of up to the fourth order. Table 2 includes all moment invariants, up to the fourth order for the NACA 2410 airfoil profile, which will be considered as the baseline design in the shape optimization example presented herein.

Table 2. Geometric moment invariants up to fourth order evaluated for NACA 2410.

$\mu_{0,0}$	$\mu_{1,0}$	$\mu_{0,1}$	$\mu_{0,2}$	$\mu_{1,1}$
1	0	0	0.0036	7.1537×10^{-4}
$\mu_{2,0}$	$\mu_{0,3}$	$\mu_{1,2}$	$\mu_{2,1}$	$\mu_{3,0}$
0.3260	3.2836×10^{-5}	-4.6849×10^{-4}	-0.0036	0.0499
$\mu_{0,4}$	$\mu_{1,3}$	$\mu_{3,1}$	$\mu_{2,2}$	$\mu_{4,0}$
2.6985×10^{-5}	1.2810×10^{-5}	7.8598×10^{-4}	-4.0455×10^{-4}	0.2297

One may easily observe from Table 2 that, when considering moment invariants, only second-order moments and above can actually be used in the combined geometry and moment vector, $\boldsymbol{p}(\mathbf{v}_{\tilde{\boldsymbol{\vartheta}}}, \boldsymbol{\mu}(\mathbf{v}_{\tilde{\boldsymbol{\vartheta}}}))$ or $\boldsymbol{p}(\boldsymbol{\vartheta})$ which was introduced in Section 2.3, since $\mu_{(0)} = 1$ and $\mu_{(1)} = (0, 0)$ for all designs.

3.2. Construction of Latent Spaces

To evaluate and analyze the effectiveness of the proposed method, latent spaces with varying design/shape signature vectors, SSVs, and discretization type are considered. The combined geometry/moments' SSVs considered in this study for each shape discretization along with the corresponding latent space notation are presented in Table 3:

Table 3. Design vectors and corresponding latent spaces for each considered geometry discretization.

Geometry only	$\boldsymbol{p}(\boldsymbol{\vartheta}_{-1})$	$\mathcal{U}_{(-1)}$
Geometry and second moments	$\boldsymbol{p}(\boldsymbol{\vartheta}_{2})$	$\mathcal{U}_{(2)}$
Geometry and third moments	$\boldsymbol{p}(\boldsymbol{\vartheta}_{3})$	$\mathcal{U}_{(3)}$
Geometry and fourth moments	$\boldsymbol{p}(\boldsymbol{\vartheta}_{4})$	$\mathcal{U}_{(4)}$
Geometry and second to third moments	$\boldsymbol{p}(\boldsymbol{\vartheta}_{2-3})$	$\mathcal{U}_{(2-3)}$
Geometry and second to fourth moments	$\boldsymbol{p}(\boldsymbol{\vartheta}_{2-4})$	$\mathcal{U}_{(2-4)}$

The efficiency of the generated latent spaces is measured by the achieved dimensionality reduction, whereas their quality is assessed using the criteria discussed in Section 2.4.1. Specifically, we begin by evaluating the achieved space-dimension reduction, depicted in Figures 3 and 4. We then measure the diversity and robustness of these spaces (as can be seen in Figures 5 and 6, respectively), followed by their ability to reconstruct, or even improve upon optimal designs acquired from the initial design space; see Table 4 and Figures 7 and 8.

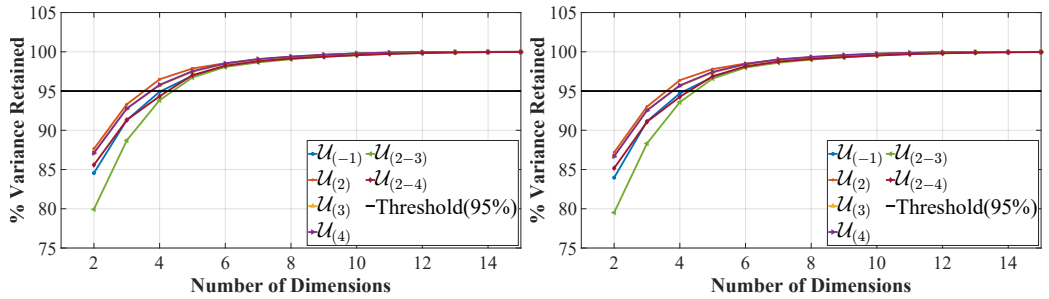

(**a**) Uniform spacing (parametric domain) (**b**) Cosine spacing

(**c**) Curvature-based spacing (**d**) Uniform spacing (physical domain)

Figure 3. Percentage of variance retained in each latent space versus the number of KL-modes employed in its construction. The horizontal black line indicates the 95% variance threshold.

With regard to efficiency, we count the number of KL-modes needed to retain a given percentage of variance from the original space. Specifically, in Figure 3, the percentage of variance achieved for each discretization and SSV against the number of employed KL-modes is plotted. If we set the variance threshold to 95% and count the number of modes required to achieve this level of variance for each SSV and discretization type, we obtain the results depicted in Figure 4. As one may observe in Figure 4, we achieve a significant dimensional reduction in the original space, i.e., from 17 dimensions[5] down to 4 or 5 dimensions while retaining 95% of variance exhibited in the original space. Furthermore, the inclusion of moments in the SSV has a slight beneficial effect in all discretizations studied, but the last one, i.e., uniform spacing at the physical domain. However, if we closely examine Figure 3d, we see that, although the inclusion of moments for this discretization type negatively affects the achieved variance, the difference is almost negligible and therefore by slightly modifying the percentage threshold, we could easily claim that the dimension of the latent space for this case is equal to four, regardless of whether moments are included or not. A similar picture can be drawn for the remaining discretization examined herein, with a slight positive impact on dimensionality reduction when second, third, or fourth moments are included in the shape signature vector. However, since the effect is not very pronounced, we may, in summary, claim that the best performing discretization type is the uniform spacing at the physical domain, closely followed by the three remaining discretization types with a slight positive impact, for all cases, when moments are included in the SSV. However, this comparison does not reveal the full picture and we need to look into the quality of each latent space and its capacity to be used in

design exploration and shape optimization. We subsequently examine these two aspects in Section 3.3 and Section 3.4, respectively.

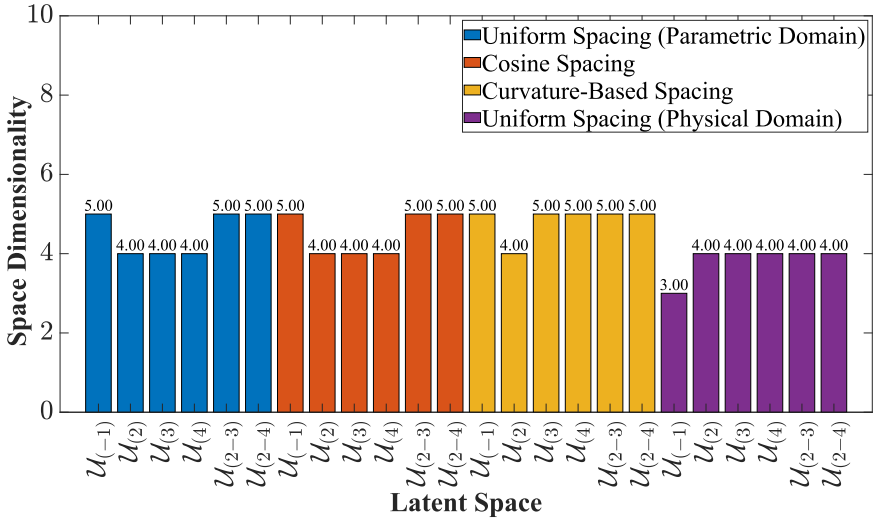

Figure 4. Dimensions required in each latent space to reach the variance threshold of 95%.

3.3. Latent Space Quality Analysis

The analysis conducted here aims to determine whether the resulting subspaces are suitable for design exploration and optimization. To this end, we assess their ability to adequately capture the underlying shape structure using the latent parameter vector **u** to generate valid and diverse geometries. The *diversity* metric is extremely important for design exploration and the capacity of the latent space to produce novel designs as it measures the difference between shapes included the latent space, as described in Section 2.4.1. *Robustness*, or shape validity, measures the percentage of invalid shapes residing in the latent space, and, as mentioned before, we ideally aim for latent spaces that eliminate or at least minimize the percentage of invalid designs. Needless to say, both quality metrics are important for shape optimization as both the existence of diverse designs as well as the absence of invalid designs have a positive impact on design optimization. To assess these quality metrics, we perform five random Monte Carlo samplings with 10,000 parameter vectors from each latent space. Subsequently, we estimate the *Robustness* with the average percentage of shapes with invalid geometries appearing in each sampling, whereas diversity is estimated by measuring the average distance between designs as described in Section 2.4.1. The acquired estimates for all discretization types and employed SSVs are presented in Figure 5 for diversity and in Figure 6 for robustness.

The estimated maximum diversity for each examined latent space, measured via Equation (17), is shown in Figure 5. In all cases the estimated values correspond to rich latent spaces as they clearly surpass the mean value of 2.6 corresponding to the original space, and approach or even surpass its maximum diversity value of 5.01. Therefore, we can state that the examined latent spaces are sufficiently rich, with diverse and novel designs, regardless of the discretization type or employed SSV. However, some slight differences among discretization types can be observed. Specifically, the curvature-based discretization produces a slightly less diverse latent space, and this result can be justified by the fact that this discretization exhibits a concentration of points in the area near the leading edge with a small number of points distributed along the remaining foil profile, as can be seen in Figure 2c. This effectively limits the exhibited shape diversity in the area of the leading edge. The remaining discretization types have a more balanced distribution of points along the profile which benefits shape diversity, as demonstrated in Figure 5. Finally, as can be easily observed in the same figure, the inclusion of moments in the shape signature vector has a negligible effect on the estimated diversity.

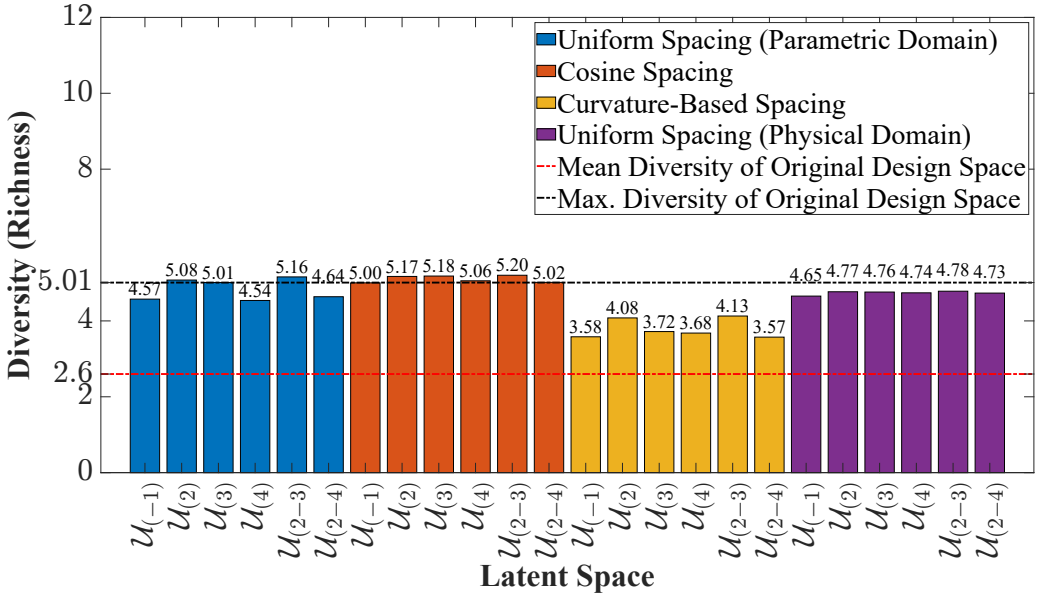

Figure 5. Diversity (richness) for each examined latent space.

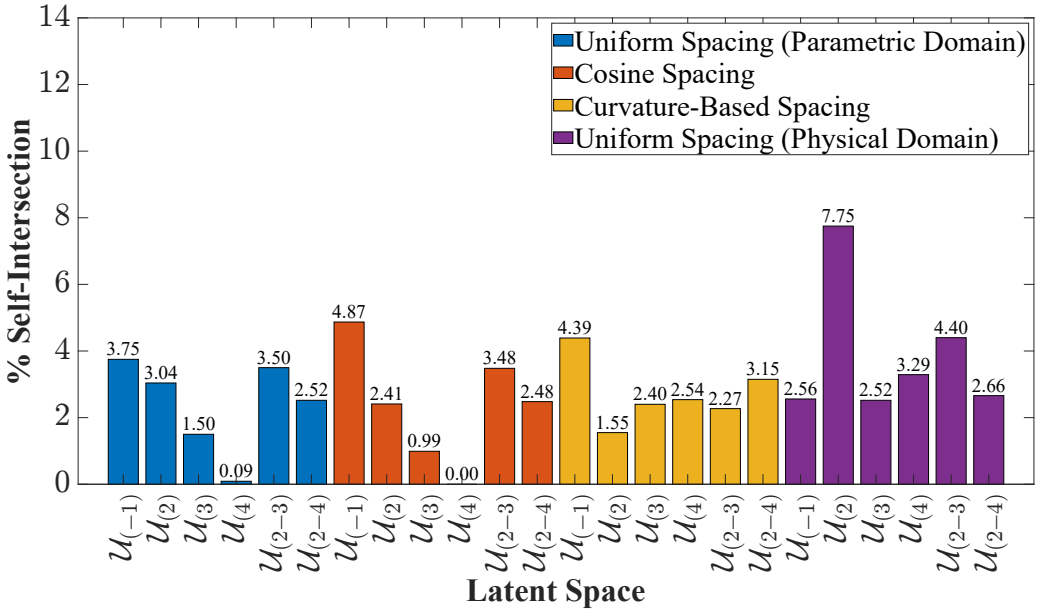

Figure 6. Percentage of invalid designs (robustness) for each examined latent space.

Although a rather balanced performance was observed with respect to diversity in the constructed latent spaces, the picture changes significantly when we examine robustness. As shown in Figure 6, both the discretization type and employed SSVs play a significant role in the existence of invalid shapes in the constructed latent spaces. Specifically, the $\mathcal{U}_{(-1)}$ latent space, constructed using only geometry as in [9], includes a percentage of invalid shapes which range from 4.87% for cosine spacing down to 2.56% when a uniform arc-length discretization is employed. For the first three discretizations, i.e., uniform (at the parametric domain), cosine and curvature-based spacing, robustness improves significantly when moments are included in the SSV, with invalid shapes being practically eliminated for the first two discretizations when fourth moments are included, as can be seen in Figure 6. This behavior, however, is not observed for the last discretization type when second moments are included in the SSV. Specifically and in this case, the percentage of invalid shapes remains practically constant across varying SSVs with the exception of an exhibited increase when second moments, either separately or in combination, are included

in the SSV. This is a rather unexpected result which requires further investigation. With the exception of the behavior exhibited for the last discretization type, our results for both diversity and robustness are in alignment with the results reported in [3] for the case of similar latent design spaces for ship hulls.

3.4. Latent Spaces in Shape Optimization

The last set of results pertains to the examination of latent spaces in performance-based shape optimization and the assessment of their capacity to reconstruct, or even improve, optimal designs acquired with the initial design space which was produced by the employed parametric model presented in Section 2.1.1. The shape optimization problem considered here is the lift optimization problem subject to a foil area constraint formulated in Equation (18). Apart from the area constraint appearing in Equation (18), the side constraints in the same equation are implemented using Equation (16). Finally, the employed optimization method is the Jaya algorithm discussed in Section 2.5.1.

As mentioned above, we perform a series of shape optimizations aiming at lift maximization under the area constraint corresponding to the NACA 2410 profile and a fixed angle of attack equal to 3°. We selected a rather low angle of attack so that we can showcase the significant shape modifications that can be achieved by latent spaces in lift maximization when drag is not taken into account. We should also stress here that the employed angle of attack does not affect the latent space construction process and any angle, or range of angles, can be readily applied when performing shape optimization with our approach. The obtained results for this series of optimizations are collected in Table 4. The lift maximization problem, when the initial design space is used, results in a reference value of the lift coefficient which is equal to 2.0518, as can be seen in the same table. All latent spaces lacking moments in their SSVs fail to attain this value and produce foil profiles with a lift coefficient value[6] ranging between 1.12 and 1.42. Three optimized foil profiles for each discretization are depicted in Figure 7, which yield the average values shown in Table 4. The reference NACA 2410 foil profile is also drawn, with a dashed black line, on the same figure for reference purposes. The results for all discretizations show a rather large dispersion with no clear tendency and inferior performances when compared to the reference optimized design. However, this behavior changes significantly when moments are included in the SSVs. As we can observe in Table 4, the lift maximization problem results in improved values when moments are added in all cases, with the latent spaces based on uniform parametric spacing and curvature-based discretizations producing results that are superior to the outcome achieved with the initial design space, see rows 1 and 3 in the same table. The latent space based on cosine spacing exhibits an improvement with the inclusion of moments and we also manage to reproduce the optimal design when fourth moments are included. However, for this case, the results are generally inferior when compared to the previous two discretizations. The remaining discretization, i.e., uniform spacing at the physical domain, also exhibits some general improvement when moments are used, but does not manage to reconstruct or improve the initial optimum design. The SSVs including moments exhibit good or superior[7] results across all discretizations, and we have indicatively included here the optimized foils shapes for $\mathcal{U}_{(4)}$ in Figure 8. As one may easily observe in the same figure, the best performing discretizations, i.e., curvature-based, cosine, and uniform parametric spacing, tend to produce a very similar foil shape (see blue-, red-, and yellow-colored curves in Figure 8) which outperforms the reference design, while the fourth discretization fails to follow the trend exhibited by the remaining latent spaces. In summary, we can state that the curvature-based discretization, which adaptively distributes points along the foil profile, exhibits the best performance, closely followed by the uniform discretization in the parametric domain. The performance of the latter discretization is justified by the fact that shape information is indirectly incorporated in the discretization since the employed parametrization is coming from the parametric model. The cosine-spacing discretization shows a rather inferior but acceptable performance, with the exception of the case where fourth moments are included in the SSV, in which optimal

behavior is also achieved. We should note here that the cosine and uniform spacing (in the physical domain) discretizations are shape-agnostic in the sense that they do not incorporate local shape features, but rely on a more general rule-set for point discretization, i.e., a dense concentration of points at the leading and trailing edge for cosine spacing and equal arc-lengths for the uniform parametrization at the physical domain. Therefore, their inferior performance can be attributed to this feature. The worst performer is clearly the last discretization (uniform spacing in the physical domain) which fails to reproduce the optimal design across all examined spaces, although a slight improvement is observed when moments are included in its SSV.

Table 4. Lift coefficient, C_L, of optimized designs for the initial and constructed latent spaces. The reported values correspond to averages from the 3 executions of the optimization algorithm.

Discretization	Initial	$\mathcal{U}_{(-1)}$	$\mathcal{U}_{(2)}$	$\mathcal{U}_{(3)}$	$\mathcal{U}_{(4)}$	$\mathcal{U}_{(2-3)}$	$\mathcal{U}_{(2-4)}$
Uniform spacing (parametric domain)	2.0518	1.4176	1.6590	**2.1210**	**2.1494**	**2.5657**	**2.7720**
Cosine spacing		1.1562	1.2220	1.5515	**2.0975**	1.2719	1.4411
Curvature-based spacing		1.2967	1.8346	**2.8000**	**2.7417**	**2.6835**	**2.2227**
Uniform spacing (physical domain)		1.1214	1.1368	1.2826	1.2210	1.1519	1.1816

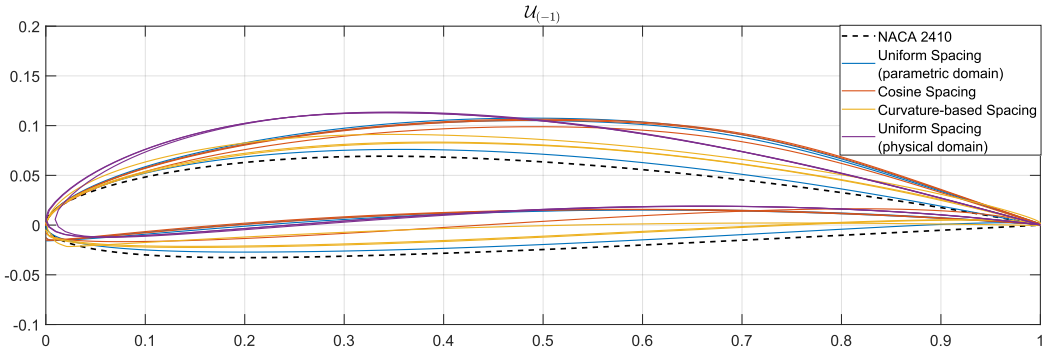

Figure 7. Optimized designs in $\mathcal{U}_{(-1)}$ latent space (no moments in the SSV).

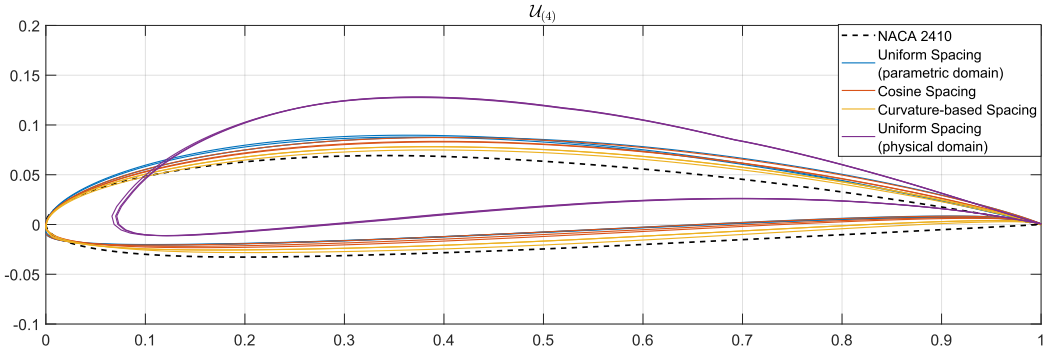

Figure 8. Optimized designs in the $\mathcal{U}_{(4)}$ latent space.

As a final note regarding shape optimization using the various latent spaces, we need to briefly discuss the challenges faced which were mainly related to handling invalid shapes in some latent spaces, as can also be seen in Figure 6. A series of additional filters and constraints were implemented, when needed, to address these problems and avoid the appearance of invalid shapes in the shape optimization procedure. Specifically, the specific problems and measures taken are collectively described below:

1. The abscissas of the first and last foil profile points were not the same for some designs, leading to performance inconsistencies when the lift coefficient was assessed using XFOIL. In most cases, the problem was a minor difference in the coordinate value,

which could be easily fixed by equating the abscissas of the two points. In the rare occasion of a big difference, the design was penalized.
2. A similar problem was faced with the ordinates of the same pair of points which was handled by penalizing the design exhibiting blunt trailing edges with a gap exceeding the maximum gap found in the UIUC database.
3. Shape irregularities including self-intersections, abrupt shape changes, and a lack of abscissa monotonicity along the upper or lower foil side. In all cases, these shape irregularities were monitored and penalized by the employed objective function.

4. Discussion and Conclusions

In this work, we studied the effects of shape discretization and geometric moments' inclusion on the performance and quality of latent design spaces produced by the generalized Karhunen–Loève expansion in the context of design space dimensionality reduction. Our results demonstrate a significant reduction in the dimensionality of the original design space while maintaining a high representational capacity and a large percentage of valid geometries that facilitate fast convergence to optimal solutions in performance-based optimization. We also demonstrated that both the type of discretization and the composition of the shape signature vector significantly affect the resulting latent spaces and their capacity to be used in design exploration and shape optimization. In summary, we may claim that shape-informed discretizations augmented with geometric moments can produce rich latent spaces which exhibit robustness and can effectively substitute the original design space when performing shape optimization. This leads to equivalent, if not better, optimal designs with a significant reduction in the computational cost as the resulting latent spaces reduce the problem's dimensionality by 60% or more.

The methodological approach and knowledge gained in this study can be expanded and employed in constructing discretizations and latent spaces that would address the problem of wings' and/or blades' design optimization, which obviously constitutes the next logical step in this line of work. As a final note, we would also like to add here that we have limited our study to steady state cases with potential flow formulation, but it would be certainly intriguing and useful to examine the applicability of this approach to more accurate flow formulations and unsteady flows that would be applicable to real-life problems and more meaningful engineering applications.

Author Contributions: Conceptualization, Z.M., K.V.K., S.K. and P.D.K.; methodology, Z.M., K.V.K., S.K. and P.D.K.; software, Z.M. and K.V.K.; validation, Z.M. and K.V.K.; formal analysis, Z.M. and S.K.; resources, K.V.K.; data curation, K.V.K.; writing—original draft preparation, Z.M. and K.V.K.; writing—review and editing, Z.M., K.V.K., S.K. and P.D.K.; supervision, K.V.K. and P.D.K.; project administration, K.V.K.; funding acquisition, K.V.K. All authors have read and agreed to the published version of the manuscript.

Funding: This work received funding from: Nazarbayev University, Kazakhstan, under the Faculty Development Competitive Research Grants Program 2022-2024: "Shape Optimization of Free-form Functional surfaces using isogeometric Analysis and Physics-Informed Surrogate Models—SOFFA-PHYS", Grant Award Nr. 11022021FD2927, PI: K.V. Kostas, and the European Union's Horizon-2020 Research and Innovation Programme under the Marie Skłodowska-Curie grant agreement No. 860843—"GRAPES: Learning, Processing and Optimising Shapes", PI: P.D. Kaklis.

Institutional Review Board Statement: Not applicable.

Informed Consent Statement: Not applicable.

Data Availability Statement: The raw data required to reproduce findings in this work are available from Zahid Masood, upon email request (zahid.masood@nu.edu.kz).

Conflicts of Interest: The authors declare no conflict of interest. The funders had no role in the design of the study; in the collection, analyses, or interpretation of data; in the writing of the manuscript; or in the decision to publish the results.

Notes

[1] After excluding some inappropriate or almost identical designs, a base set with 1263 foil designs was identified. For each of these base designs, five random shape perturbations around them were generated, leading to $6 \times 1263 = 7578$ foil designs.

[2] Excluding, of course, the case of a coincident pair of points at the trailing edge.

[3] If we split the foil curve in two parts using the points corresponding to the minimum and maximum coordinate, each part should behave as a graph of function.

[4] XFOIL version 6.99, Mark Drela, MIT, USA URL: https://web.mit.edu/drela/Public/web/xfoil/ accessed on 1 May 2023.

[5] Recall that we need to use 17 parameters of the foil parametric model to represent the dataset within Kulfan tolerance; see also Section 2.1.1.

[6] These values correspond to averages of the lift coefficient values corresponding to optimum shapes acquired by the successive executions of the optimization algorithm at a fixed 3° angle of attack.

[7] To a lesser extent when only second moments are included.

References

1. Khan, S.; Goucher-Lambert, K.; Kostas, K.; Kaklis, P. ShipHullGAN: A generic parametric modeller for ship hull design using deep convolutional generative model. *Comput. Methods Appl. Mech. Eng.* **2023**, *411*, 116051. [CrossRef]
2. Harries, S.; Abt, C.; Brenner, M. Upfront CAD—Parametric modeling techniques for shape optimization. In *Advances in Evolutionary and Deterministic Methods for Design, Optimization and Control in Engineering and Sciences*; Springer: Cham, Switzerland, 2019; pp. 191–211.
3. Khan, S.; Awan, M.J. A generative design technique for exploring shape variations. *Adv. Eng. Inform.* **2018**, *38*, 712–724. [CrossRef]
4. Bellman, R.E. *Dynamic Programming*; Princeton University Press: Princeton, NJ, USA, 2010.
5. Montgomery, D.C.; Weatherby, G. *Factor Screening Methods in Computer Simulation Experiments*; Technical Report; Institute of Electrical and Electronics Engineers (IEEE): Piscataway, NJ, USA, 1979.
6. Khan, S.; Kaklis, P. From regional sensitivity to intra-sensitivity for parametric analysis of free-form shapes: Application to ship design. *Adv. Eng. Inform.* **2021**, *49*, 101314. [CrossRef]
7. Sobol, I.M. Global sensitivity indices for nonlinear mathematical models and their Monte Carlo estimates. *Math. Comput. Simul.* **2001**, *55*, 271–280. [CrossRef]
8. Bengio, Y.; Courville, A.; Vincent, P. Representation learning: A review and new perspectives. *IEEE Trans. Pattern Anal. Mach. Intell.* **2013**, *35*, 1798–1828. [CrossRef] [PubMed]
9. Diez, M.; Campana, E.F.; Stern, F. Design-space dimensionality reduction in shape optimization by Karhunen–Loève expansion. *Comput. Methods Appl. Mech. Eng.* **2015**, *283*, 1525–1544. [CrossRef]
10. Khan, S.; Kaklis, P.; Serani, A.; Diez, M.; Kostas, K. Shape-supervised Dimension Reduction: Extracting Geometry and Physics Associated Features with Geometric Moments. *Comput.-Aided Des.* **2022**, *150*, 103327. [CrossRef]
11. He, X.; Yan, S.; Hu, Y.; Niyogi, P.; Zhang, H.J. Face recognition using laplacianfaces. *IEEE Trans. Pattern Anal. Mach. Intell.* **2005**, *27*, 328–340.
12. Belkin, M.; Niyogi, P. Laplacian eigenmaps for dimensionality reduction and data representation. *Neural Comput.* **2003**, *15*, 1373–1396. [CrossRef]
13. Yu, W.; Wang, R.; Nie, F.; Wang, F.; Yu, Q.; Yang, X. An improved locality preserving projection with ℓ_1-norm minimization for dimensionality reduction. *Neurocomputing* **2018**, *316*, 322–331. [CrossRef]
14. Chen, W.; Chiu, K.; Fuge, M.D. Airfoil design parameterization and optimization using Bézier generative adversarial networks. *AIAA J.* **2020**, *58*, 4723–4735. [CrossRef]
15. Du, X.; He, P.; Martins, J.R. A B-spline-based generative adversarial network model for fast interactive airfoil aerodynamic optimization. In Proceedings of the AIAA Scitech 2020 Forum, Orlando, FL, USA, 6–10 January 2020; p. 2128.
16. Kedward, L.; Allen, C.B.; Rendall, T. Gradient-limiting shape control for efficient aerodynamic optimization. *AIAA J.* **2020**, *58*, 3748–3764. [CrossRef]
17. Li, J.; Bouhlel, M.A.; Martins, J.R. Data-based approach for fast airfoil analysis and optimization. *AIAA J.* **2019**, *57*, 581–596. [CrossRef]
18. UIUC Applied Aerodynamics Group. UIUC Airfoil Coordinates Database. 2023. Available online: https://m-selig.ae.illinois.edu/ads/coord_database.html (accessed on 1 February 2023).
19. Li, J.; Zhang, M.; Martins, J.R.; Shu, C. Efficient aerodynamic shape optimization with deep-learning-based geometric filtering. *AIAA J.* **2020**, *58*, 4243–4259. [CrossRef]
20. Li, J.; Zhang, M. On deep-learning-based geometric filtering in aerodynamic shape optimization. *Aerosp. Sci. Technol.* **2021**, *112*, 106603. [CrossRef]
21. Kostas, K.; Ginnis, A.; Politis, C.; Kaklis, P. Shape-optimization of 2D hydrofoils using an Isogeometric BEM solver. *Comput.-Aided Des.* **2017**, *82*, 79–87. [CrossRef]
22. Kostas, K.; Amiralin, A.; Sagimbayev, S.; Massalov, T.; Kalel, Y.; Politis, C. Parametric model for the reconstruction and representation of hydrofoils and airfoils. *Ocean. Eng.* **2020**, *199*, 107020. [CrossRef]

23. Masters, D.A.; Poole, D.J.; Taylor, N.J.; Rendall, T.; Allen, C.B. Impact of Shape Parameterisation on Aerodynamic Optimisation of Benchmark Problem. In Proceedings of the 54th AIAA Aerospace Sciences Meeting, Kissimmee, FL, USA, 5–9 January 2016. [CrossRef]
24. Masters, D.A.; Taylor, N.J.; Rendall, T.C.S.; Allen, C.B.; Poole, D.J. Geometric Comparison of Aerofoil Shape Parameterization Methods. *AIAA J.* **2017**, *55*, 1575–1589. [CrossRef]
25. Kulfan, B.; Bussoletti, J. Fundamental Parametric Geometry Representations for Aircraft Component Shapes. In Proceedings of the 11th AIAA/ISSMO Multidisciplinary Analysis and Optimization Conference, Portsmouth, VA, USA, 6–8 September 2006.
26. Kulfan, B.M. Universal Parametric Geometry Representation Method. *J. Aircr.* **2008**, *45*, 142–158. [CrossRef]
27. Piegl, L.; Tiller, W. *The Nurbs Book*, 2nd ed.; Springer: Berlin/Heidelberg, Germany, 1997.
28. Drela, M.; Giles, M. Viscous-inviscid analysis of transonic and low Reynolds number airfoils. *AIAA* **1987**, *25*, 1347–1355. [CrossRef]
29. Drela, M. XFOIL: An Analysis and Design System for Low Reynolds Number Airfoils. In *Low Reynolds Number Aerodynamics. Lecture Notes in Engineering*; Mueller, T., Ed.; Springer: Berlin/Heidelberg, Germany, 1989; Volume 54.
30. Kostas, K.V.; Manousaridou, M. Machine-Learning-Enabled Foil Design Assistant. *J. Mar. Sci. Eng.* **2023**, *11*, 1470. [CrossRef]
31. Bronstein, A.M.; Bronstein, M.M.; Kimmel, R. *Numerical Geometry of Non-Rigid Shapes*; Springer Science & Business Media: Berlin/Heidelberg, Germany, 2008.
32. Xu, D.; Li, H. Geometric moment invariants. *Pattern Recognit.* **2008**, *41*, 240–249. [CrossRef]
33. Cignoni, P.; Rocchini, C.; Scopigno, R. Metro: Measuring error on simplified surfaces. *Computer Graphics Forum* **1998**, *17*, 167–174. [CrossRef]
34. Rao, R. Jaya: A simple and new optimization algorithm for solving constrained and unconstrained optimization problems. *Int. J. Ind. Eng. Comput.* **2016**, *7*, 19–34. [CrossRef]
35. Masood, Z.; Khan, S.; Qian, L. Machine learning-based surrogate model for accelerating simulation-driven optimisation of hydropower Kaplan turbine. *Renew. Energy* **2021**, *173*, 827–848. [CrossRef]
36. Degertekin, S.O.; Lamberti, L.; Ugur, I.B. Sizing, layout and topology design optimization of truss structures using the Jaya algorithm. *Appl. Soft Comput.* **2018**, *70*, 903–928. [CrossRef]
37. Degertekin, S.; Yalcin Bayar, G.; Lamberti, L. Parameter free Jaya algorithm for truss sizing-layout optimization under natural frequency constraints. *Comput. Struct.* **2021**, *245*, 106461. [CrossRef]
38. Li, B.; Li, Z.; Yang, P.; Xu, J.; Wang, H. Modeling and optimization of the thermal-hydraulic performance of direct contact heat exchanger using quasi-opposite Jaya algorithm. *Int. J. Therm. Sci.* **2022**, *173*, 107421. [CrossRef]
39. Atrevi, D.F.; Vivet, D.; Duculty, F.; Emile, B. A very simple framework for 3D human poses estimation using a single 2D image: Comparison of geometric moments descriptors. *Pattern Recognit.* **2017**, *71*, 389–401. [CrossRef]
40. Jin, P.; Xie, B.; Xiao, F. Multi-moment finite volume method for incompressible flows on unstructured moving grids and its application to fluid-rigid body interactions. *Comput. Struct.* **2019**, *221*, 91–110. [CrossRef]